Letter

Signatures of electronic correlations and spin-susceptibility anisotropy in nuclear magnetic resonance

Stephen Carr,[1,2] Charles Snider,[1] D. E. Feldman,[1,2] Chandrasekhar Ramanathan,[3] J. B. Marston,[1,2] and V. F. Mitrović[1]

[1]*Department of Physics, Brown University, Providence, Rhode Island 02912-1843, USA*

[2]*Brown Theoretical Physics Center, Brown University, Providence, Rhode Island 02912-1843, USA*

[3]*Department of Physics and Astronomy, Dartmouth College, Hanover, New Hampshire 03755, USA*

(Received 13 October 2021; revised 20 April 2022; accepted 14 July 2022; published 29 July 2022)

We present a methodology for probing the details of electronic susceptibility through minimally invasive nuclear magnetic resonance techniques. Specifically, we classify electron-mediated long-range interactions in an ensemble of nuclear spins by revealing their effect on simple spin echo experiments. We find that the pulse strength and applied field orientation dependence of these spin echo measurements resolves the spatial extent and anisotropy of electronic spin susceptibility. This Letter provides an alternate explanation to NMR results in superconducting and magnetically ordered systems. The methodology has direct applications for sensing and characterizing emergent electronic phases.

DOI: 10.1103/PhysRevB.106.L041119

Nuclear magnetic resonance (NMR) traditionally measures dissipation using the temperature dependence of the spin-lattice relaxation rates (T_1) or spin-spin relaxation rates (T_2) [1–4]. Changes in dissipation rates can be compared to models for electron-nuclear or phonon-nuclear interactions, allowing for the microscopic observation of electronic phases. This standard approach for NMR as an experimental probe provides relationships between electronic spin susceptibility at high-symmetry points and the dissipation rates. NMR is an attractive tool for probing electronic ground state properties as it uses low-frequency excitations relative to electronic energies. Recently identified quantum phases of matter may encode details of their intricate structure into NMR responses in ways that lie outside this current paradigm.

It is not uncommon in NMR studies of strongly correlated materials to observe unusual time-asymmetric features from standard spin echo protocols. These are typically classified as experimental artifacts, often attributed to an uncontrolled phase transition as strong rf pulses can cause electronic heating in the sample [5–8]. Inspired by these observations, we provide an alternate explanation for such unconventional signals by investigating the time evolution of nuclear spins with electron-mediated interactions on a two-dimensional (2D) lattice. When the interaction couples nuclei more than a few lattice lengths apart, clear signatures emerge in NMR spectra during pulse angle sweeps, including evidence of an anisotropic electronic structure. The radial form and range of the interaction is also partially recoverable from a careful analysis of the spin dynamics. As the details of the nuclear interaction are inherited from the electronic spin susceptibility, one can determine many features of electronic spin-spin correlation previously inaccessible by NMR. In this Letter we demonstrate how to extract the range and anisotropy of electronic spin correlations through a series of simple NMR experiments in correlated phases of solid matter.

Long-range interactions between magnetic particles through conduction electrons have been studied previously [9–13], but a theory for an interacting lattice of spinors with long-range couplings is underdeveloped. The general model for coupled nuclear spins is well understood [14], with many packages available for treatment of the full Hilbert space (limited to $N \approx 20$ spins) [15–18]. Truncated Liouville space representations can handle up to $N \approx 1000$ spins [19–21], but we find that even this is not large enough to capture the emergent properties from long-range electronic correlations. Classical treatments with only nearest-neighbor coupling have found good agreement with quantum methods [22], and the agreement generally improves as the number of interacting neighbors increases [23]. A well-known example of a successful mean-field treatment is the theory of multiple echoes from long-range nuclear dipole interactions in solid ^{3}He [24].

We consider tens of thousands of spins and treat the interactions at the mean-field level [25,26]. Our simulations are performed on an $n_x \times n_y$ square lattice of unit length with spin-$\frac{1}{2}$ nuclei [Fig. 1(a)] with periodic boundary conditions and a Lorentzian distribution of resonant frequencies with linewidth Γ. We perform small Δt updates on each spin in the ensemble, with Δt chosen small enough to prevent any error from approximation of the Hamiltonian matrix exponential during time propagation [see Supplemental Material (SM) [27], Sec. II]. To achieve a spin echo, at $t = 0$ a θ-strength I^x pulse brings all the spins out of alignment with B_z and towards the xy plane. After a time $\tau = 5/\Gamma$, a 2θ-strength I^y pulse rotates them about the y axis. When $\theta = 90^\circ$ this achieves a perfect 180° rotation of the spins, canceling the accumulated phases from the variations in ν and forming a spin echo at $t = 2\tau$. We present the in-plane net magnetization of the spin ensemble, $\bar{M}^{xy}(t) = \bar{M}^x(t) + i\bar{M}^y(t)$, and its Fourier

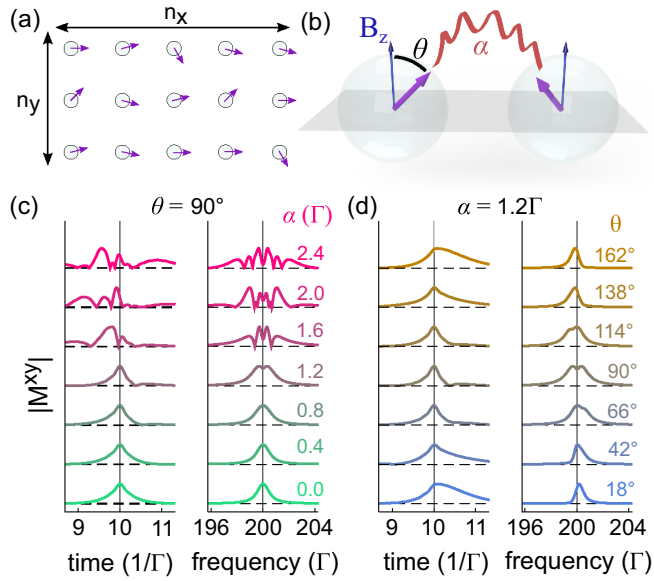

FIG. 1. (a) Top-down view of a square lattice of nuclear spins of size $n_x \times n_y$. (b) The interaction between nuclei depends on a characteristic strength α. By varying the strength of the first applied pulse the expected angle θ between the spins and the constant B_z can be modified. (c) Average planar magnetization from spin echo simulations, in both the time and frequency domain, for a fixed θ and varying α, and (d) vice versa.

transform (see SM, Sec. IV) in Figs. 1(c) and 1(d). We use the notation $\bar{M}$ for the global net magnetization, to distinguish from a local magnetization M.

Applying second-order perturbation theory to the hyperfine interaction of strength Δ, here assumed to be a diagonal tensor, between electrons and nuclei leads to an effective spin-spin interaction bilinear in the nuclear spins and quadratic in the hyperfine strength [28,29]. The effective Hamiltonian for the spin-spin interaction between nuclei takes the form

$$H_I(i,j) \propto \Delta^2 \boldsymbol{I}_i^\dagger \chi(R_i - R_j)\boldsymbol{I}_j, \tag{1}$$

where χ is the spin susceptibility of the electrons and $\boldsymbol{I} = (I^x, I^y, I^z)$ are the nuclear spin operators. The form of Eq. (1) avoids the assumption of an isotropic Fermi liquid, and also makes explicit the proportional relationship between χ and the nuclear-nuclear coupling. Making a mean-field approximation of the interaction in Eq. (1), we keep only the diagonal elements of χ to obtain

$$H_{\rm mf}(i) = -\nu_i I_i^z - \sum_{d=x,y,z} \alpha_d I_i^d M_i^d, \tag{2}$$

with ν_i the resonant frequency of the noninteracting spin, M_i^d the mean magnetization along the dth axis seen by a spinor at lattice site i from the other spins, and α_d the effective strength of the hyperfine electron-mediated coupling along that spin axis, as illustrated in Fig. 1(b). This direct relation between χ and α is more complicated for nondiagonal hyperfine tensors, and in this case independent experimental measurement of the form of the hyperfine tensor is necessary before χ can be reconstructed from our methodology of measuring α. We also note that for short-range interactions (where $\boldsymbol{M}$ is sensitive only to the nearest neighboring nuclei, for example) this mean-field approximation is not reliable, but it should become more accurate as the range of the interaction is increased and the interaction averages over more nuclei. We treat the spin operators as unitless and absorb all relevant physical constants into ν and α, whose frequencies will be given in units of the linewidth Γ. Time values will be in units of Γ^{-1}.

We expect the introduction of the $\boldsymbol{I}^2$ operator to break the even time symmetry of $|\bar{M}_{xy}(t)|$ around the spin echo. As the strength of the $\boldsymbol{I}^2$ term depends on the average magnetization when the interaction is long range, it leads to an explicit time dependence in the Hamiltonian. The time evolution of the spins can be estimated by $d\boldsymbol{H}/d\boldsymbol{I}$, which acts as an effective torque on each spinor. For the noninteracting case, $d\boldsymbol{H}/d\boldsymbol{I} = -\nu\hat{z}$, a constant, and so if the initial distribution of spins is frequency symmetric the resulting echo will be time symmetric. As $\boldsymbol{M}(t)$ acts as a nonconstant torque, it allows for the breaking of time symmetry in the spin echo. As seen for $\alpha = 1.2$ in Fig. 1(c), the ramping strength of the interaction as t approaches the echo time causes the postecho shoulder to have a different shape than the pre-echo shoulder, and for larger α values a remnant magnetization from the initial decay causes significant time asymmetry.

We begin with the simplest isotropic infinite-range interaction form, $\boldsymbol{M}_i = \bar{\boldsymbol{M}} = \sum_j \langle \boldsymbol{I}_j \rangle / N$ and $\alpha_d \equiv \alpha$. This uses the net magnetization of the entire ensemble (N spins) as the local magnetization when determining $H_{\rm mf}$, leaving α and the pulse angle θ as the only unfixed parameters. The role of the coupling strength α is investigated first in Fig. 1(c). Weak α values (<1) show a nearly perfect spin echo in both the time and frequency domain. As α grows, time-asymmetric echoes occur. The interaction causes the most significant changes to the spin evolution near the echo and shortly after the initial pulse [free induction decay (FID)]. For $\alpha < 1.2$, the only noticeable effect on $M(t)$ occurs near the echo time, showing up as a small postecho shoulder. At larger α values, the interactions cause significant ringing even during the FID (see SM). In Fig. 1(d), the effect of different pulse strengths on the spin echo are compared. There are many reductions in the magnetization near 10 MHz reminiscent of spectral hole burning, so the signatures of strong electron-mediated nuclear coupling could easily be misattributed to overpumping the system [8].

To remove the assumption of an isotropic interaction, we introduce the axis-dependent couplings, $\alpha_z \neq \alpha_x = \alpha_y \equiv \alpha_{xy}$, motivated by anisotropy in the electronic spin susceptibility: $\chi^{zz} \neq \chi^{xx}, \chi^{yy}$. This can occur in layered materials [30] or be caused by spontaneous electronic nematicity [31–35]. Figure 2 investigates three different conditions for the anistropic interaction: $\alpha_{xy} = 0$, $\alpha_z = 0$, and $\alpha_{xy} \neq \alpha_z$. For $\alpha_{xy} = 0$ [Fig. 2(a)] the interaction simply introduces an additional I^z term, increasing or decreasing the average resonant frequency of the ensemble. Understanding the distribution of spins in the absence of interactions reveals how θ shifts the resonant frequency.

We have derived the values of $\bar{\boldsymbol{M}}$ in the noninteracting case exactly in the SM's Sec. V, but here we outline the argument for $\bar{M}^z$ by representing the spins as a vector of magnitude

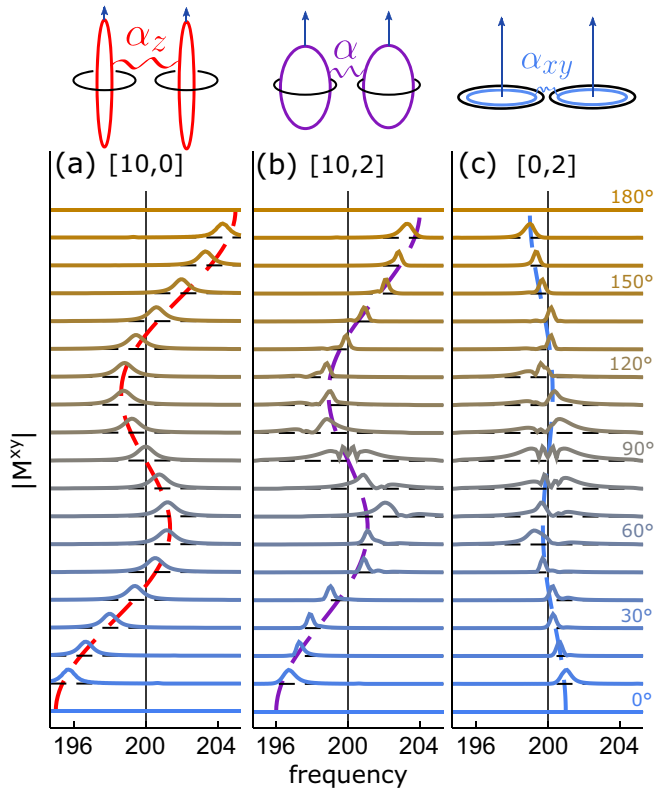

FIG. 2. Pulse angle (θ) dependence of the NMR spectra for different aspect ratios of the effective spin-spin interaction, $[\alpha_z, \alpha_{xy}]$ in units of Γ. The S function $[(\alpha_{xy} - \alpha_z)/4](\cos\theta + \cos 3\theta)$ is given by the dashed line for each aspect ratio.

1/2 (Fig. 3). The first θ pulse moves all the spins an angle θ off the z axis, where they then precess because of B_z and trace out a ring centered along the z axis. Assuming the time between each pulse (τ) is long enough to ensure that the spins are uniformly distributed, the second 2θ pulse then rotates the now uniform ring of spins an additional angle θ away from the z axis. The average z component of the spins just after the 2θ pulse is given by the average of the maximal and minimal z-component values of the tilted ring, $\cos\theta$ and $\cos 3\theta$, respectively. The z component is unchanged under further time evolution by B_z. Therefore $\bar{M}^z$ during the spin echo

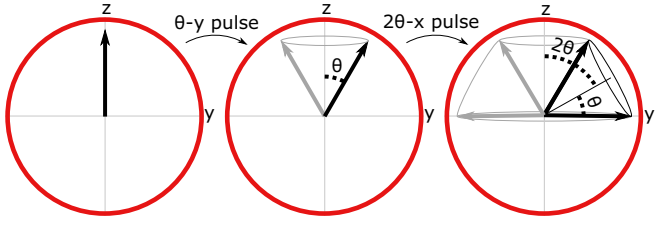

FIG. 3. Distribution of nuclear spins in the absence of the spin-spin interaction during a $[\theta, 2\theta]$ pulse sequence. After each pulse, the updated spin distribution is given by a dark black line, and the distribution a short time after the pulse is given by the gray outlines. The distribution just before the 2θ pulse traces out a cone, and so the last figure considers a rotated cone instead of a rotated arrow.

is $(\alpha_z/4)(\cos\theta + \cos 3\theta)$, which we denote as an S function, and in agreement with the frequency shift observed in the simulations. Although Fig. 3 only shows the case for $\theta < 90°$, our derivation of the average $\bar{M}^z$ value holds for all θ.

Considering instead $\alpha_z = 0$ [Fig. 2(c)], one can estimate the magnitude of the in-plane magnetization at $t = 2\tau$. A simple geometric argument is not possible for the in-plane magnetization, but the exact treatment yields $\bar{M}^x = 0$ and $\bar{M}^y = (\alpha_{xy}/2)\sin^3\theta$ (see SM, Sec. V). Because each spin is acted upon by I^z from B_z, and I^x and I^y from the interaction, behavior beyond a simple frequency shift is expected. The multipeak behavior is most pronounced when the magnitude of the in-plane magnetization is largest, e.g., near $\theta = 90°$. There is also an S-function shift caused by the in-plane interaction, with magnitude $(\alpha_{xy}/4)$, which is due to the weak α_{xy} torque applied to the z component of the spins after the 2θ pulse (see SM, Sec. VIII). For the third case where $\alpha_{xy} \neq \alpha_z$ [Fig. 2(b)] the S function's amplitude depends on the difference of α_z and α_{xy}, and the presence of α_z does not remove the multiple peaks generated by α_{xy} near $\theta = 90°$.

Inverting the argument for the results of Fig. 2, in a laboratory setting the pulse variation experiment could be performed under different chosen directions for the B_z fields relative to the sample's crystalline axis. If the nuclei-nuclei coupling is mostly isotropic, the resulting NMR signals should not depend on the placement of the z axis (in the absence of any other effects). If the coupling is stronger along one axis than the other two, a clear S function such as that of Fig. 2(a) will occur along a specific direction of the applied field, while if it is weaker along one axis, an inverted S function with severe hole-burning-like features should occur [Fig. 2(c)].

Figure 2(b) shows qualitative similarities to experimental spectra from a superconducting phase [8]. Namely, at low power (low θ) the observed peaks were at a low frequency, but as the power increases (increasing θ) they shift to higher frequencies and show unusual nonmonotonic behavior, similar to the S function. Mapping power (dB) to a pulse angle (deg) is challenging in experiment, especially when we predict large reductions in the signal near 90°, so more theoretical and experimental work is necessary. The most direct approach to investigate the origin of the spectral shifts is to repeat experiments with greatly increased repetition time, as long repetition times minimize the accumulation of heat in the sample and would distinguish spin-spin interactions from heating effects. The evolution of the echo shape and position as a function of the pulse power and orientation of the applied field permit us to reverse engineer details of this material's electronic spin susceptibility.

Our work also allows for the determination of the spatial extent of electron-electron correlations. In real materials, each spinor will feel a local contribution from nearby nuclei, not a global average of the magnetization. Between different materials and quantum spin phases, the type of radial decay in the susceptibility and its characteristic correlation length will vary. To investigate this variation, we define the local magnetization $\boldsymbol{M}_i$ felt by a nucleus at site r_i as the sum

$$\boldsymbol{M}_i = \sum_j K(r_{ij})\,\langle \boldsymbol{I}_j \rangle, \tag{3}$$

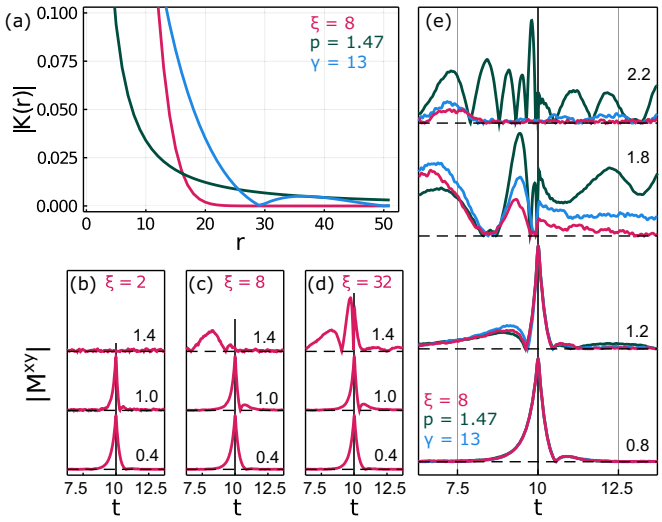

FIG. 4. (a) Absolute value of the three magnetization kernels, K: Gaussian (red) with $\xi = 8$, power (green) with $p = 1.47$, and RKKY (blue) with $\gamma = 13$. (b)–(d) Time-domain spin echoes for an isotropic Gaussian kernel with a short-, medium-, and long-range ξ (time in units of Γ^{-1}). (e) Simulated time-domain spin echoes for the isotropic kernels with medium length scale as given in (a) for increasing interaction strength. All three curves are identical for $\alpha_{\text{eff}} = 0.8$. In (b)–(e), $\theta = 90^\circ$ and the total effective interaction, α_{eff} in Eq. (4), is given in black on the right of each set of simulated spin echo curves in units of Γ.

with K a radial kernel for the interaction. We study three choices of K here. First, is a short-range Gaussian that depends on a correlation length ξ, $K(r) = e^{-(r/\xi)^2}$, motivated by the susceptibility expected from a gapped spin excitation. Second, is a long-range form given by a power p, $K(r) = r^{-p}$, motivated by a gapless spin excitation. Finally, we study the Ruderman-Kittel-Kasuya-Yosida (RKKY) form expected from spin interactions in a simple metal [28,29] which is also dependent on a length γ, $K(x) = x^{-4}(x\cos x - \sin x)$ for $x = 2(r/\gamma)$. In Fig. 4(a) the three functional forms for K are plotted using parameters that yield similar length scales, for comparison.

Spin echo results identical to those of Figs. 1 and 2 are possible in this more realistic model if α and the length-scale parameters ξ, p, or γ are chosen appropriately (see SM, Sec. VI). The key parameter is the average effective interaction

$$\alpha_{\text{eff}} \equiv \sum_{d=x,y,z} \frac{\alpha_d}{3} \sum_{ij} K(r_{ij}), \tag{4}$$

which is an integral of the interaction over the lattice and averaged over the three spin-spin spatial dimensions. We find that a local interaction produces similar echoes to that of the global magnetization studied earlier, as long as the α used in the global case is similar to α_{eff} of the local one and the range of the interaction is sufficiently long. In Figs. 4(b)–4(d), simulations with an isotropic ($\alpha_d = \alpha$) Gaussian functional for three values of ξ are shown. At the small value of $\xi = 2$, the spin echo acts similarly to the infinite-range model for weak α_{eff}. But as the interaction increases, the coupling to neighboring spins becomes so strong that extreme variations in the local effective magnetization occur throughout the lattice, destroying the echo. For intermediate values ($\xi = 8$) similar behavior is observed, but now the critical α_{eff} for complete destruction of an echo is larger. When the correlation length is much larger than the lattice parameter ($\xi = 32$), the echo is identical to the results of the infinite-range coupling even for large α_{eff}. Therefore, the effective strength of the coupling (α_{eff}) can be determined if an echo occurs, and the higher its value the longer range the electronic spin-spin correlations must be. To estimate the critical minimal value of ξ for a given α_{eff} in a three-dimensional lattice, we take $\xi^{2/3} \approx 4, 10$ lattice lengths, for the intermediate- and long-range values respectively.

Echoes caused by interactions with similar α_{eff} but different isotropic radial forms are shown in Fig. 4(e). We see that although all three curves show similar qualitative trends, there are small details that distinguish them. For example, in the pre-echo shoulder ($t = 7.5$) the RKKY form always has the highest $\bar{M}^{xy}(t)$ value, followed by the Gaussian, and then the power form. Similarly, in the postecho shoulder ($t = 12.5$), the power form yields the largest $\bar{M}^{xy}(t)$ and the Gaussian form the smallest. At the largest α_{eff} value in Fig. 4(e), these trends no longer hold because the echoes have disappeared for the Gaussian and RKKY forms. The RKKY form is an oscillating power-law decay, with its nodes partially canceling long-range contributions and making it act as a short-range interaction in our model. The power law balances local versus average magnetization and prevents a complete breakdown of the spin echo phenomena.

Careful evaluation of NMR responses provides valuable insight into systems with long-range electronic spin correlations. We demonstrate that pulse-induced spectral line shifts could be caused not only by external effects quenching an electronic phase, but also by the electronic phase itself. There are two important conditions that must be satisfied by the electronic spin susceptibility for this effect to occur. First, the integral of the electron-mediated nuclear interaction strength (a_{eff}) must be similar to or larger than the material's natural linewidth. Second, this interaction must be relatively strong over a large number of nuclei, such that the spin-spin interactions lead to an effective spin memory in the system instead of the T_2 decay that occurs when the interaction is only among nearest neighbors. Our work encourages careful consideration of any NMR result in a strongly correlated system, be it a conventional solid or an artificial atomic lattice. Clear signatures of nematic (anisotropic) ordering can be revealed by changing the pulse strength and orientation of the applied field. Moreover, the methodology developed here gives insight into the radial form and range of electronic correlations. We hope that extensions of this work can ultimately lead to the ability to reverse engineer the full electronic susceptibility from simple NMR spectral measurements.

We thank Mladen Horvatić for helpful comments. This work was supported by the National Science Foundation under Grant No. OIA-1921199. The calculations were conducted using computational resources and services at the Center for Computation and Visualization, Brown University.

[1] C. H. Pennington, D. J. Durand, C. P. Slichter, J. P. Rice, E. D. Bukowski, and D. M. Ginsberg, NMR measurement of the exchange coupling between Cu(2) atoms in $YBa_2Cu_3O_{7-\delta}$ ($T_c = 90$ K), Phys. Rev. B **39**, 274 (1989).

[2] C. H. Pennington and C. P. Slichter, Theory of Nuclear Spin-Spin Coupling in $YBa_2Cu_3O_{7-\delta}$, Phys. Rev. Lett. **66**, 381 (1991).

[3] M. Horvatić, T. Auler, C. Berthier, Y. Berthier, P. Butaud, W. G. Clark, J. A. Gillet, P. Ségransan, and J. Y. Henry, NMR investigation of single-crystal $YBa_2Cu_3O_{6+x}$ from the underdoped to the overdoped regime, Phys. Rev. B **47**, 3461 (1993).

[4] V. F. Mitrović, H. N. Bachman, W. P. Halperin, A. P. Reyes, P. Kuhns, and W. G. Moulton, Pseudogap in $YBa_2Cu_3O_{7-\delta}$ from NMR in high magnetic fields, Phys. Rev. B **66**, 014511 (2002).

[5] K. Ishida, M. Manago, K. Kinjo, and Y. Maeno, Reduction of the ^{17}O Knight shift in the superconducting state and the heat-up effect by NMR pulses on Sr_2RuO_4, J. Phys. Soc. Jpn. **89**, 034712 (2020).

[6] A. Pustogow, Y. Luo, A. Chronister, Y.-S. Su, D. A. Sokolov, F. Jerzembeck, A. P. Mackenzie, C. W. Hicks, N. Kikugawa, S. Raghu, E. D. Bauer, and S. E. Brown, Constraints on the superconducting order parameter in Sr_2RuO_4 from Oxygen-17 nuclear magnetic resonance, Nature (London) **574**, 72 (2019).

[7] I. Vinograd, S. P. Edwards, Z. Wang, T. Kissikov, J. K. Byland, J. R. Badger, V. Taufour, and N. J. Curro, Inhomogeneous Knight shift in vortex cores of superconducting FeSe, Phys. Rev. B **104**, 014502 (2021).

[8] V. F. Mitrović, G. Koutroulakis, M. Klanjšek, M. Horvatić, C. Berthier, G. Knebel, G. Lapertot, and J. Flouquet, Comment on "Texture in the Superconducting Order Parameter of $CeCoIn_5$ Revealed by Nuclear Magnetic Resonance", Phys. Rev. Lett. **101**, 039701 (2008).

[9] S. Ouazi, J. Bobroff, H. Alloul, M. Le Tacon, N. Blanchard, G. Collin, M. H. Julien, M. Horvatić, and C. Berthier, Impurity-Induced Local Magnetism and Density of States in the Superconducting State of $YBa_2Cu_3O_7$, Phys. Rev. Lett. **96**, 127005 (2006).

[10] J. A. Sobota, D. Tanasković, and V. Dobrosavljević, RKKY interactions in the regime of strong localization, Phys. Rev. B **76**, 245106 (2007).

[11] A. Bermudez, F. Jelezko, M. B. Plenio, and A. Retzker, Electron-Mediated Nuclear-Spin Interactions between Distant Nitrogen-Vacancy Centers, Phys. Rev. Lett. **107**, 150503 (2011).

[12] H. Prüser, P. E. Dargel, M. Bouhassoune, R. G. Ulbrich, T. Pruschke, S. Lounis, and M. Wenderoth, Interplay between the Kondo effect and the Ruderman–Kittel–Kasuya–Yosida interaction, Nat. Commun. **5**, 5417 (2014).

[13] R. G. Mohammadi and A. G. Moghaddam, Anisotropic RKKY interactions mediated by $j = \frac{3}{2}$ quasiparticles in half-Heusler topological semimetals, Phys. Rev. B **101**, 075421 (2020).

[14] J. Robert and L. Wiesenfeld, Magnetic anisotropic interactions of nuclei in condensed matter, Phys. Rep. **86**, 363 (1982).

[15] M. Bak, J. T. Rasmussen, and N. C. Nielsen, SIMPSON: A general simulation program for solid-state NMR spectroscopy, J. Magn. Reson. **147**, 296 (2000).

[16] Z. Tošner, R. Andersen, B. Stevensson, M. Edén, N. C. Nielsen, and T. Vosegaard, Computer-intensive simulation of solid-state NMR experiments using SIMPSON, J. Magn. Reson. **246**, 79 (2014).

[17] M. Veshtort and R. G. Griffin, SPINEVOLUTION: A powerful tool for the simulation of solid and liquid state NMR experiments, J. Magn. Reson. **178**, 248 (2006).

[18] H. Hogben, M. Krzystyniak, G. Charnock, P. Hore, and I. Kuprov, Spinach – a software library for simulation of spin dynamics in large spin systems, J. Magn. Reson. **208**, 179 (2011).

[19] J.-N. Dumez, M. C. Butler, and L. Emsley, Numerical simulation of free evolution in solid-state nuclear magnetic resonance using low-order correlations in Liouville space, J. Chem. Phys. **133**, 224501 (2010).

[20] A. Karabanov, D. Wiśniewski, I. Lesanovsky, and W. Köckenberger, Dynamic Nuclear Polarization as Kinetically Constrained Diffusion, Phys. Rev. Lett. **115**, 020404 (2015).

[21] A. Karabanov and W. Köckenberger, Spectral Green's-function method in driven open quantum dynamics, Phys. Rev. A **103**, 012224 (2021).

[22] C. Tang and J. S. Waugh, Dynamics of classical spins on a lattice: Spin diffusion, Phys. Rev. B **45**, 748 (1992).

[23] T. A. Elsayed and B. V. Fine, Effectiveness of classical spin simulations for describing NMR relaxation of quantum spins, Phys. Rev. B **91**, 094424 (2015).

[24] G. Deville, M. Bernier, and J. M. Delrieux, Nmr multiple echoes observed in solid ^3He, Phys. Rev. B **19**, 5666 (1979).

[25] C. Snider, S. Carr, D. E. Feldman, C. Ramanathan, J. B. Marston, and V. F. Mitrović (unpublished).

[26] The repository for code used in this work is available at https://github.com/stcarr/SpinEchoSim.

[27] See Supplemental Material at http://link.aps.org/supplemental/10.1103/PhysRevB.106.L041119 for information on the model and results of our simulations, which includes Refs. [36–38].

[28] M. A. Ruderman and C. Kittel, Indirect exchange coupling of nuclear magnetic moments by conduction electrons, Phys. Rev. **96**, 99 (1954).

[29] K. Yosida, Magnetic properties of Cu-Mn alloys, Phys. Rev. **106**, 893 (1957).

[30] P. A. Joy and S. Vasudevan, Magnetism in the layered transition-metal thiophosphates MPS_3 (M = Mn, Fe, and Ni), Phys. Rev. B **46**, 5425 (1992).

[31] I. J. Pomeranchuk, On the stability of a Fermi liquid, J. Exptl. Theoret. Phys. (U.S.S.R.) **35**, 524 (1958) [Sov. Phys. JETP **8**, 361 (1958)].

[32] S. A. Kivelson, E. Fradkin, and V. J. Emery, Electronic liquid-crystal phases of a doped Mott insulator, Nature (London) **393**, 550 (1998).

[33] C. J. Halboth and W. Metzner, d-Wave Superconductivity and Pomeranchuk Instability in the two-Dimensional Hubbard Model, Phys. Rev. Lett. **85**, 5162 (2000).

[34] V. Oganesyan, S. A. Kivelson, and E. Fradkin, Quantum theory of a nematic Fermi fluid, Phys. Rev. B **64**, 195109 (2001).

[35] E. Fradkin, S. A. Kivelson, M. J. Lawler, J. P. Eisenstein, and A. P. Mackenzie, Nematic Fermi fluids in condensed matter physics, Annu. Rev. Condens. Matter Phys. **1**, 153 (2010).

[36] G. Lindblad, On the generators of quantum dynamical semigroups, Commun. Math. Phys. **48**, 119 (1976).

[37] V. Gorini, A. Kossakowski, and E. C. G. Sudarshan, Completely positive dynamical semigroups of N-level systems, J. Math. Phys. **17**, 821 (1976).

[38] M. Am-Shallem, A. Levy, I. Schaefer, and R. Kosloff, Three approaches for representing Lindblad dynamics by a matrix-vector notation, arXiv:1510.08634.